Dynamical Transition in a Small Helical Peptide and Its Implication for Vibrational Energy Transport

Ellen H. G. Backus,[†] Robbert Bloem,[‡] Rolf Pfister,[‡] Alessandro Moretto,[§] Marco Crisma,[§] Claudio Toniolo,[§] and Peter Hamm*[,‡]

FOM Institute for Atomic and Molecular Physics, 1098 SJ Amsterdam, The Netherlands, Physikalisch-Chemisches Institut, Universität Zürich, CH-8057 Zürich, Switzerland, and Institute of Biomolecular Chemistry, Padova Unit, CNR, Department of Chemistry, University of Padova, I-35131 Padova, Italy

Received: May 26, 2009; Revised Manuscript Received: July 14, 2009

The two-dimensional infrared spectrum of an octameric helical peptide in chloroform was measured as a function of temperature. Isotope labeling of the carbonyl group of one of the amino acids was used to obtain information for an isolated vibration. The antidiagonal width of the 2D-IR signal, which is a measure of the homogeneous dephasing time T_2, is constant from 220 to 260 K (within experimental error), and increases steeply above. The homogeneous dephasing time of the carbonyl vibration is attributed to the flexibility of the system and/or its immediate surrounding. The system undergoes a dynamical transition at about 270 K, with similarities to the protein dynamical transition. Furthermore, the temperature dependence of the antidiagonal width strongly resembles that of the efficiency of vibrational energy transport along the helix, which has been studied in a recent paper (*J. Phys. Chem. B* **2008**, *112*, 15487). The connection between the two processes, structural flexibility and energy transport mechanism, is discussed.

Introduction

Vibrational energy or heat transport plays a key role in the functioning of many molecular systems. For example, excess energy after ultrafast photochemical reactions has to be removed efficiently from photoactive proteins. Furthermore, it has been speculated that the regulatory and active sites of an allosteric protein actually communicate through distinct vibrational energy pathways.[1] Also, for the development of molecular electronic devices, understanding the mechanism of energy transport through a molecular system would be helpful. Therefore, vibrational energy transport through different molecular systems, e.g., a bridged azulene−anthracene compound,[2] single amino acids,[3] self-assembled monolayers of long-chain hydrocarbon molecules,[4] model membranes,[5,6] and proteins,[7−9] has been studied.

Recently,[10] we have suggested that the vibrational energy transport properties of a short peptide helix in solution can be modulated by tuning the structural flexibility of the molecule. We studied the vibrational energy transport through a model helix at different temperatures after dumping energy at one end of the molecule through the internal conversion of an electronically excited chromophore. At low temperature, vibrational energy transport is inefficient and ballistic-like. Above ca. 270 K, the vibrational energy transport efficiency rises steeply and the mechanism changes from ballistic- to diffusive-like.

Conventional IR and NMR spectroscopies suggested that the change in mechanism at ca. 270 K is connected to a dynamical transition; i.e., the helix is relatively stiff below 270 K and becomes increasingly more flexible above. An earlier NMR experiment on another Aib-rich peptide also hinted to a sudden increase of the backbone flexibility at ca. 270 K, thereby facilitating the transition between the left- and right-handed 3_{10}-helix.[11] Furthermore, accompanying molecular dynamics (MD) simulations revealed that the backbone dihedral fluctuations increase in a step-like manner around that temperature.[10] Such a dynamical transition could explain the peculiar temperature dependence of vibrational energy transport properties. Vibrational energy can efficiently travel through the helix only through low-frequency modes, because only these modes tend to be delocalized over larger parts of the helix.[9] The transport through these low-frequency modes will be to a certain extent ballistic. Energy in higher frequency modes, on the other hand, can only travel once it has relaxed into one of the low-frequency delocalized modes. At high temperature, the intrasite vibrational energy redistribution (IVR) is facilitated by the large flexibility of the molecular system, whereas this step is very slow at low temperatures. Consequently, at low temperature, the vibrational energy transport is inefficient, as only the energy initially deposited in low-frequency modes will be transported. That small fraction, however, will be transported in essentially a ballistic manner, since it is transported through strongly delocalized, phonon-like modes. At higher temperature, in contrast, the transport becomes more efficient, because IVR within individual sites now becomes possible, albeit it is still rate-limiting. IVR is a dissipative process, and as such, the dynamics is diffusive-like. This picture is in accordance with the results from a recent simulation study on a toy model that mimics the distribution of normal modes in the peptide and at the same time is small enough to model vibrational energy transport fully quantum-mechanically.[12]

We have noted in ref 10 that the biphasic behavior of the vibrational energy transport efficiency resembled that of proteins around the so-called protein dynamical transition (also known as the glass transition), that occurs at ca. 200 K in aqueous solution.[13−17] The physical origin of this transition, however, is still discussed controversially. Many researchers favor the picture that the glass transition is slaved by the properties of the solvent,[18−20] while others believe it is intrinsic to the

[†] FOM Institute for Atomic and Molecular Physics.
[‡] Universität Zürich.
[§] University of Padova.

10.1021/jp904905d CCC: $40.75
Published on Web 09/15/2009

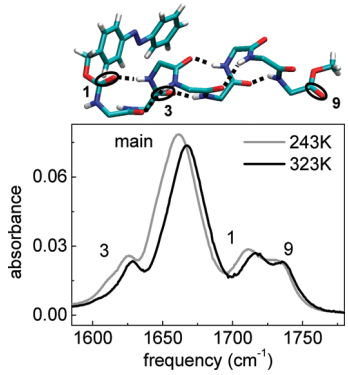

Figure 1. FTIR absorption spectra in the C═O spectral region at 243 and 323 K, taken from ref 10. Top panel: X-ray diffraction structure of the peptide backbone and terminal protection groups (amino acid side chains are not shown).[29] Intramolecular hydrogen bonds are represented by dashed lines. Labels 1, 3, and 9 count C═O sites with increasing distance from the azobenzene moiety.

protein.[21] In any case, the molecules are trapped in various, essentially harmonic energy basins below the glass temperature T_g, whereas they are free to structurally diffuse above. The glass transition is very well established for proteins in aqueous solution, but recently a dynamical transition with apparently very similar properties has also been observed for a very small peptide by THz spectroscopy.[22] From the theory side, the concept of a glass transition has been applied to characterize the folding of small peptides that do form well-defined secondary structures.[23] Also in our previous works,[10] we had presented both experimental and theoretical signatures that were used in exactly the same manner as an indicator for a glass transition in proteins.[15,17]

In order to further support the interpretation of our previous results,[10] we report here on the homogeneous dephasing rate (T_2) of a marker vibrational mode as a function of temperature. From all IR spectroscopic signatures, the homogeneous dephasing rate responds the most sensitive to the glass transition in proteins.[24−27] That is, the homogeneous dephasing rate of proteins in aqueous solution is only weakly temperature dependent below the glass transition and rises steeply above. Also, for a dye dissolved in a glass forming mixture, the same biphasic behavior has been observed.[28] In the present paper, we use 2D-IR spectroscopy to measure the effective homogeneous dephasing rate of a spectrally isolated carbonyl vibration (by isotope labeling), and we will show that its temperature dependence resembles that of the vibrational energy transport efficiency.

Our model system, used already before,[10,29,30] is an octameric peptide, dPAZ-Aib-^{13}C-Ala-Aib$_6$-OMe (dPAZ, fully deuterated 4-(phenyldiazenyl-benzyloxycarbonyl; OMe, methoxy; see top panel of Figure 1 for the 3D-structure). It consists of mainly α-aminoisobutyric acid (Aib),[31,32] which is a strong 3_{10}-helix former especially in chloroform.[33,34] To be site selective, one of the amino acids has a ^{13}C═O labeled group, shifting the vibrational frequency to a lower value so that it is separated from the other amide I vibrations. Because ^{13}C(carbonyl)-alanine (Ala) is more readily available commercially than ^{13}C(carbonyl)-Aib, we used the former for isotope labeling. Disturbing the Aib$_8$ sequence by one guest residue (Ala), however, does not destabilize the 3_{10}-helix significantly.[29,31,32]

Materials and Methods

The experiments were performed on an actively phase-stabilized 2D-IR photon-echo setup described in detail before.[35,36] Briefly, IR pulses (1640 cm^{-1}, fwhm 170 cm^{-1}) were generated by a Ti:S pumped OPA combined with a difference frequency mixing stage. Subsequently, the IR pulses were split in three strong excitation pulses (∼0.3 μJ each) and two weak ones (one used as the local oscillator, LO, and one as the reference). The third order polarization emitted in the $-k_1 + k_2 + k_3$ direction interferes with the LO. After dispersion in a spectrometer (Triax Series), they were imaged onto 32 pixels of an array detector (Infrared Associates) with a spectral resolution of 2.4 cm^{-1}. The reference, passing the sample at a slightly different position, was imaged on another line of the detector in order to correct for shot-to-shot fluctuations. Purely absorptive 2D-IR spectra were obtained by summing up the rephasing and nonrephasing diagrams, measured by interchanging the time ordering of pulses 1 and 2. All beams were polarized in parallel. A reference pump−probe spectrum, used for phasing of the 2D-IR spectra, was recorded with pulse 3 as the pump pulse and the LO as the probe pulse, while blocking beams 1 and 2.

The 2D data were collected with time steps of 25.34 fs (undersampling, the vibrational period of amide I is ∼20 fs) up to 6.8 ps for both the rephasing and nonrephasing configurations, resulting in a spectral resolution after Fourier transformation of ∼5 cm^{-1} along the pump axis. With zero padding, we enhanced the resolution on the pump axis to 2.5 cm^{-1}, thereby matching the resolution on the probe axis (2.4 cm^{-1}). In this manner, the antidiagonal cuts can be obtained with better accuracy. The waiting time T was 300 fs.

Phasing of the 2D-IR spectra was performed by comparing the projection of the purely absorptive 2D spectrum onto the probe frequency axis to a pump−probe spectrum recorded after broadband excitation (projection slice theorem).[37] Since the signal for the isotope labels is quite small, we used the main band at ca. 1660 cm^{-1} for determining the phase (the spectral phase is basically constant over the IR pulse; we only changed the grating of the spectrometer to swap between the two spectral regions).

Synthesis of the peptide and its structural characterization have been described in detail in ref 29. Briefly, deuterated PAZ−Aib−OH was synthesized by nitrating toluene-d_8 to *p*-nitrotoluene, oxidizing to *p*-nitrobenzoic acid, reducing with zinc to *p*-aminobenzoic acid, and then making the methyl ester using methanol and thionyl chloride. Reduction of the methyl ester with lithium−aluminum−deuteride[38] leads to the fully deuterated *p*-aminobenzyl alcohol. Nitrosobenzene-d_5 was obtained by reduction of nitrobenzene-d_5, as described in ref 39. Coupling these two deuterated compounds and covalently linking the resulting alcohol to Aib was performed in the same way (via dPAZ−Cl), as reported in refs 40 and 41. Peptide synthesis was performed in solution by activating the carboxyl function with 1-[3-(dimethylamino)propyl]-3-ethylcarbodiimide and 7-aza-1-hydroxy-1,2,3-benzotriazole.[42] The peptide was dissolved in chloroform (Sigma-Aldrich, used without further purification) at a concentration of ∼3 mM. The sample was held between two CaF_2 windows, separated by a 100 μm spacer, placed inside a temperature controlled liquid nitrogen flow cell cryostat.

Results

The linear absorption spectra at two different temperatures are shown in Figure 1. The bands at 1625, 1660, 1720, and 1730 cm^{-1} are assigned to the isotopically labeled amide I vibration, the main amide I band (originating from all of the nonlabeled amino acids), the vibration of the urethane group linking the azobenzene moiety, and that of the C-terminal ester

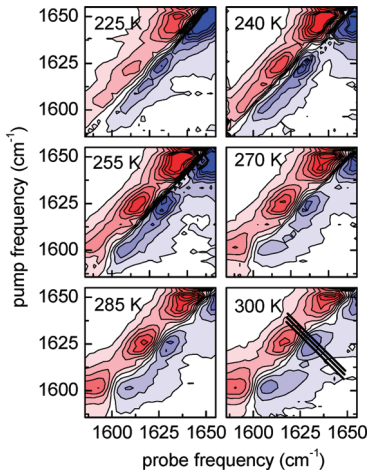

Figure 2. Purely absorptive 2D-IR spectra at six different temperatures. The diagonal peak at ~1605 cm^{-1} originates from the solvent or impurities in it. The band at 1625 cm^{-1}, the isotopically labeled amide I vibration, shows a clear decrease of the antidiagonal width with decreasing temperature. In the upper right corner, the main band starts to appear. The black lines in the spectrum for 300 K illustrate the antidiagonal cuts used for Figures 3 and 4.

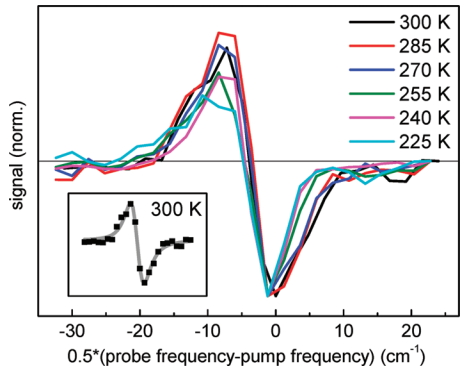

Figure 3. Antidiagonal cut for the different temperatures normalized and shifted to the antidiagonal at 300 K. The inset shows the antidiagonal cut at 300 K (black squares) together with the fit (gray line) with a sum of two Lorentzian functions: one for the positive excited state absorption signal, and one for the negative bleach and stimulated emission signal.

group, respectively.[10,29] Upon lowering the temperature, the bands shift to lower frequency.

In Figure 2, 2D spectra from 225 to 300 K are shown. All spectra reveal three diagonal peaks at 1608, 1625, and 1655 cm^{-1}. The peak at 1608 cm^{-1} originates from $CHCl_3$ or from some pollution in it (potentially water or the stabilizer ethanol), because this peak is also visible in a 2D spectrum of only $CHCl_3$ (data not shown). The peaks at 1625 and 1655 cm^{-1} come from the isotope labeled amide C═O and from the main band, respectively. Comparing the different temperatures with each other, we can observe that the bands shift slightly (most obvious for the main band) to lower frequency by lowering the temperature, in agreement with the linear absorption spectra depicted in Figure 1. Moreover, the antidiagonal width of the bands, especially that of the isotopically labeled amide I vibration at 1625 cm^{-1}, decreases with decreasing temperature, while the diagonal width remains essentially the same.

In the simplest picture (see the Discussion below), the diagonal width reflects the total line width of the transition (which in principle could already be deduced from the linear absorption spectra, see Figure 1), whereas the antidiagonal width measured at early waiting times (T = 300 fs) is related to the

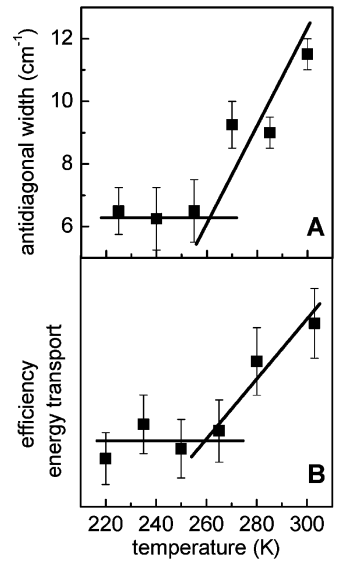

Figure 4. Temperature dependence: (A) the antidiagonal width of the isotopically labeled carbonyl vibration compared with (B) the vibrational energy transport efficiency. The latter is adapted from ref 10. The lines are to guide the eyes.

homogeneous line width.[43] In other words, the convolution of the homogeneous and inhomogeneous linewidths is temperature independent, but the homogeneous contribution increases as the temperature rises.

In Figure 3, the antidiagonal cuts taken at the maximum of the negative peak for the isotope labeled carbonyl amide band in the 2D plot (see, e.g., the center black line in Figure 2 for 300 K) are depicted for all temperatures. The line width of the negative peak decreases with decreasing temperature and is constant below 260 K (within experimental error). At the same time, the intensity of the positive peak seems to decrease, which has no physical meaning; this is because we take an antidiagonal cut, whereas the anharmonically shifted 1−2 transition is horizontally (and not diagonally) shifted to lower frequencies. To quantify the information on their line width, the antidiagonals are fitted with a sum of two Lorentzian functions: one for the high-frequency side of the positive excited state absorption signal, and one for the negative bleach and stimulated emission signal (see inset of Figure 3). For every temperature, the line width for the negative peak from the fit is then averaged over three antidiagonal cuts around the peak of the band (see the three black lines in Figure 2 for 300 K). Figure 4a shows the result. The antidiagonal width (full width at half-maximum) is more or less constant at ~6 cm^{-1} until 260 K and then increases with temperature to ~12 cm^{-1} at 300 K. The temperature dependence of the homogeneous line width qualitatively resembles the temperature dependence of the vibrational energy transport efficiency, as discussed in ref 10 and plotted here in Figure 4b for comparison.

One comment is in order here: While very clearly the homogeneous line width increases with temperature, the signal-to-noise of the data of Figure 4a taken alone would not be sufficient to rigorously conclude that there is a transition at 270 K. A fit of the data by a linear function (not shown) reveals a rms deviation of 0.78 cm^{-1}, whereas that of a quadratic fit, a function that we consider purely phenomenological but mimics a transition, is 0.58 cm^{-1}. These numbers need to be compared to the average error bar of the data, 0.75 cm^{-1}. In that sense, the noise of the data is just at the edge to allow one distinguishing between both cases. Nevertheless, we find the

same transition temperature (i) for both the mechanism (diffusive versus ballistic) and the efficiency of vibrational energy transport (as discussed in detail in ref 10), in (ii) stationary IR and NMR spectra that hint to less persistent hydrogen bonds above that transition temperature,[10] as well as in (iii) the MD results for the fluctuation amplitude of the backbone dihedral angles.[10] It is this combination of observations that make us believe that a transition is indeed taking place at this temperature (that for sure will not be discontinuous for a finite system).

We know from the NMR measurements in our previous works that this type of peptides tends to aggregate, most likely in a head-to-tail manner.[10] The concentration in the present experiment (3 mM) is at the lower edge, and only a maximal 10% of the molecules aggregate at this dilution. We had verified in ref 10 that the vibrational energy transport efficiency shows the same temperature dependence (Figure 4b) in a concentration range from 3 to 15 mM, so we tentatively concluded that the transition is not initiated by aggregation. That conclusion is in agreement with the MD results,[10] which revealed the transition for a single peptide.

Discussion

In the framework of Kubo's stochastic theory of lineshapes,[44,45] which has been shown to provide a very good description of the dephasing of vibrational transitions in the solution phase, the 1D and 2D lineshapes can be deduced from the so-called frequency fluctuation correlation function (FFCF) $\langle\omega(t)\omega(0)\rangle$, where $\omega(t)$ is the deviation of the instantaneous frequency of a probe vibration (the isotopically labeled amide C═O vibration in our case) from its mean. As the environment pushes and pulls on that carbonyl group, the instantaneous frequency varies a little bit, giving rise to line broadening.[46] For solution phase systems, one consistently finds that the FFCF decays in a distinctly biphasic manner with a so-called inertial component on a 100 fs time scale and a significantly slower diffusive component on a picosecond or even much slower time scale (the latter depending on, e.g., the viscosity of the solvent). 2D-IR spectroscopy has been widely used to extract the FFCF.[36,47,48] The slower, diffusive process could, in principle, be observed by 2D-IR spectroscopy when varying the waiting time T. In the present case, we had fixed this waiting time to $T = 300$ fs, the earliest time to completely avoid temporal overlap of the laser pulses. Hence, we essentially freeze in the diffusive motion and we can think of it as quasi-inhomogeneous (i.e., "static" on the 300 fs time scale). For the fast inertial component, on the other hand, one finds for most vibrational transitions that it is in the so-called motional narrowing limit, in which case it is characterized by a single parameter, the homogeneous line width $\Gamma_{\mathrm{hom}} = (\pi c T_2)^{-1}$. In simple words, the antidiagonal width of a 2D spectrum then corresponds to this homogeneous width Γ_{hom}.[43] This is the hole-burning picture of 2D-IR spectroscopy; i.e., excitation at a certain frequency along the pump-frequency axis burns a hole, the width of which is the homogeneous width.

The lifetime (T_1) contribution to the homogeneous width is an issue that needs to be discussed. Vibrational relaxation of amide I vibrations is relatively fast (≈1 ps),[30,49,50] and as such contributes significantly to the homogeneous line width (≈5 cm^{-1}). However, from the literature, it is known that the temperature dependence of pure dephasing T_2^* is much stronger than that of T_1: for myoglobin−CO in trehalose, pure dephasing T_2^* varies roughly 1 order of magnitude, while T_1 is roughly constant.[25,26] Also, for the amide I band of myoglobin, T_1 varies only 30% over 100 K.[49] As we see an increase of 100% for the homogeneous width over only 40 K, we conclude that the dominant contribution to the temperature dependence of the homogeneous width originates from pure dephasing T_2^*.

In essence, the homogeneous line width of the carbonyl vibration measures the amount of fast fluctuations with correlation times in the order of $\tau_c \approx 100$ fs (slower components would appear as quasi-inhomogeneous for the short waiting time we had chosen). It is exactly these fast components that will also most efficiently facilitate IVR. That is, the relaxation rate between two vibrational modes k_{IVR} is governed by the spectral density of the force−force autocorrelation function exerted by the surrounding, evaluated at the frequency that equals the energy gap $\Delta\varepsilon$ between two modes:[46]

$$k_{\mathrm{IVR}} \propto \int_0^\infty \mathrm{d}t \cos(\Delta\varepsilon \cdot t)\langle F(t)F(0)\rangle \qquad (1)$$

Although there is certainly not a simple one-to-one relationship between the forces giving rise to IVR (eq 1) and those giving rise to dephasing through the FFCF, it is clear that the origin of both effects is the same, i.e., the fast fluctuations of the surrounding. From eq 1, we can deduce that the inertial fluctuation component with a typical correlation time of $\tau_c \approx$ 100 fs will most efficiently facilitate IVR over energy gaps smaller than roughly $1/(c \cdot \tau_c) \approx 300$ cm^{-1}.[50] As a single site (Aib) in our helix has 26 intrasite normal modes below ca. 1700 cm^{-1} (all modes but the split-off part from the CH and NH stretch vibrations), the average energy spacing between two subsequent modes will be 65 cm^{-1}. These energy gaps can easily be bridged by this sort of fast solvent fluctuations. Hence, at least on a very qualitative level, we can understand that homogeneous dephasing (Figure 4a) and the vibrational energy transport efficiency (Figure 4b) should indeed go in parallel. This discussion intrinsically assumes that the rate-limiting step of the latter is in fact IVR within the individual sites, as shown in a recent simulation study.[12]

Conclusion

Two conclusions can be drawn from this work. First, this paper sheds new light on the dynamical transition which so far has been observed mainly for proteins.[13−19,21] That is, we can reproduce many of the observations for this small peptide that have been made before in the context of the protein dynamical transition. For example, in ref 10, we have reported a kink in the amide I frequency shift at the transition temperature, that has been reported also for proteins.[15] In addition, MD simulations[10] of the peptide revealed a step-like increase of the fluctuation amplitude of the backbone dihedral angles in the exact same manner as that for the much larger protein myoglobin.[17] In the present work, we have shown that the homogeneous line width, which is believed to respond most sensitively to a glass transition, follows precisely the same trend as in proteins.[27] This observation is in agreement with recent results from THz spectroscopy, which investigated the dynamical transition of various proteins or peptides in either the folded or denatured state.[22] It has been shown that the dynamical transition does not require any secondary or tertiary structure; it just requires a minimal length of at least five amino acids. We tentatively assign the different transition temperature we observe, ≈270 K, in contrast to ≈200 K for peptides and proteins in aqueous solution, to the different solvent we used. The bulk solvent, chloroform, does not undergo any phase transition at 270 K; it remains a liquid in this temperature range (in contrast to many experiments performed on proteins, where the glass transition occurs at a lower temperature, 190 K). Nevertheless,

the different transition temperatures suggest that a solvation shell of a certain size contributes to the dynamical transition. In full accordance with ref 22, we therefore conclude that the concept of a dynamical transition is much more general than commonly assumed. However, it should be noted that although MD simulations can indeed reveal an increase of the homogeneous line width with temperature, they seem not to reproduce any transition behavior, neither for the energy transport efficiency nor the homogeneous line width.[51]

Second, we clearly show that it is the flexibility of the molecular system, measured through the homogeneous dephasing time of one vibrational probe, which modulates the energy transport efficiency and also its mechanism. That is, at low temperature, the molecule is stiff and the fluctuations of the system are slow, so that only the vibrational energy already present in delocalized low-frequency modes is transported through the helix in a ballistic manner. At higher temperatures, the molecule becomes more flexible, and the increasing fluctuations facilitate intrasite IVR so that the vibrational energy present in high-frequency modes can relax into transporting low-frequency modes. The relaxation of energy is now the rate-limiting step resulting in a diffusive type of vibrational energy transfer. This might prove to be a concept of how one, or Nature, can regulate vibrational energy transport properties of molecular devices under these extreme conditions by engineering the flexibility of their components.

Acknowledgment. The authors want to thank Gerhard Stock for numerous very instructive discussions on the topic, and Sean Garrett-Roe as well as Roland Zehnder for their extraordinary help in making the experiments possible. The work has been supported by The Netherlands Organisation for Scientific Research (NWO) through a postdoc fellowship to EHG Backus and the Swiss National Science Foundation (Grant 200020-115877).

References and Notes

(1) Leitner, D. M. *Annu. Rev. Phys. Chem.* **2008**, *59*, 233, and references therein.
(2) Schwarzer, D.; Kutne, P.; Schröder, C.; Troe, J. *J. Chem. Phys.* **2004**, *121*, 1754.
(3) Naraharisetty, S. R. G.; Kasyanenko, V. M.; Zimmermann, J.; Thielges, M. C.; Romesberg, F. E.; Rubtsov, I. V. *J. Phys. Chem. B* **2009**, *113*, 4940.
(4) Wang, Z.; Carter, J. A.; Lagutchev, A.; Koh, Y. K.; Seong, N.-H.; Cahill, D. G.; Dlott, D. D. *Science* **2007**, *317*, 787.
(5) Deàk, J. C.; Pang, Y.; Sechler, T. D.; Wang, Z.; Dlott, D. D. *Science* **2004**, *306*, 473.
(6) Kuciauskas, D.; Wohl, C. J.; Pouy, M.; Nasai, A.; Gulbinas, V. *J. Phys. Chem. B* **2004**, *108*, 15376.
(7) Lian, T.; Locke, B.; Kholodenko, Y.; Hochstrasser, R. M. *J. Phys. Chem.* **1994**, *98*, 11648.
(8) Mizutani, Y.; Kitagawa, T. *Science* **1997**, *278*, 443.
(9) Yu, X.; Leitner, D. M. *J. Phys. Chem. B* **2003**, *107*, 1698.
(10) Backus, E. H. G.; Nguyen, P. H.; Botan, V.; Moretto, A.; Crisma, M.; Toniolo, C.; Zerbe, O.; Stock, G.; Hamm, P. *J. Phys. Chem. B* **2008**, *112*, 15487.
(11) Hummel, R. P.; Toniolo, C.; Jung, G. *Angew. Chem., Int. Ed. Engl.* **1987**, *26*, 1150.
(12) Schade, M.; Hamm, P. *J. Chem. Phys.*, **2009**, *131*, 44511.
(13) Hartmann, H.; Parak, F.; Steigemann, W.; Petsko, G. A.; Ponzi, D. R.; Frauenfelder, H. *Proc. Natl. Acad. Sci. U.S.A.* **1982**, *79*, 4967.
(14) Rasmussen, B. F.; Stock, A. M.; Ringe, D.; Petsko, G. A. *Nature* **1992**, *357*, 423.
(15) Demmel, F.; Doster, W.; Petry, W.; Schulte, A. *Eur. Biophys. J.* **1997**, *26*, 327.
(16) Ringe, D.; Petsko, G. A. *Biophys. Chem.* **2003**, *105*, 667.
(17) Moritsugu, K.; Smith, J. C. *J. Phys. Chem. B* **2006**, *110*, 5807.
(18) Vitkup, D.; Ringe, D.; Petsko, G. A.; Karplus, M. *Nat. Struct. Biol.* **2000**, *7*, 34.
(19) Tournier, A. L.; Xu, J.; Smith, J. C. *Biophys. J.* **2003**, *85*, 1871.
(20) Fenimore, P. W.; Frauenfelder, H.; McMahon, B. H.; Young, R. D. *Proc. Natl. Acad. Sci. U.S.A.* **2004**, *101*, 14408.
(21) Lee, A. L.; Wand, A. J. *Nature* **2001**, *411*, 501.
(22) He, Y.; Ku, P. I.; Knab, J. R.; Chen, J. Y.; Markelz, A. G. *Phys. Rev. Lett.* **2008**, *101*, 178103.
(23) Hansmann, U. H. E.; Onuchic, J. N. *J. Chem. Phys.* **2001**, *115*, 1601.
(24) Rella, C. W.; Kwok, A.; Rector, K.; Hill, J. R.; Schwettman, H. A.; Dlott, D. D.; Fayer, M. D. *Phys. Rev. Lett.* **1996**, *77*, 1648.
(25) Rella, C. W.; Rector, K. D.; Kwok, A.; Hill, J. R.; Schwettman, H. A.; Dlott, D. D.; Fayer, M. D. *J. Phys. Chem.* **1996**, *100*, 15620.
(26) Rector, K. D.; Engholm, J. R.; Rella, C. W.; Hill, J. R.; Dlott, D. D.; Fayer, M. D. *J. Phys. Chem. A* **1999**, *103*, 2381.
(27) Fayer, M. D. *Annu. Rev. Phys. Chem.* **2001**, *52*, 315.
(28) Lazonder, K.; Pshenichnikov, M. S.; Wiersma, D. A. *Chem. Phys. Lett.* **2007**, *449*, 255.
(29) Botan, V.; Backus, E. H. G.; Pfister, R.; Moretto, A.; Crisma, M.; Toniolo, C.; Nguyen, P. H.; Stock, G.; Hamm, P. *Proc. Natl. Acad. Sci. U.S.A.* **2007**, *104*, 12749.
(30) Backus, E. H. G.; Nguyen, P. H.; Botan, V.; Pfister, R.; Moretto, A.; Crisma, M.; Toniolo, C.; Stock, G.; Hamm, P. *J. Phys. Chem. B* **2008**, *112*, 9091.
(31) Karle, I. L.; Balaram, P. *Biochemistry* **1990**, *29*, 6747.
(32) Toniolo, C.; Crisma, M.; Formaggio, F.; Peggion, C. *Biopolymers* **2001**, *60*, 396.
(33) Toniolo, C.; Benedetti, E. *Trends Biochem. Sci.* **1991**, *16*, 353.
(34) Bolin, K. A.; Millhauser, G. L. *Acc. Chem. Res.* **1999**, *32*, 1027.
(35) Volkov, V.; Schanz, R.; Hamm, P. *Opt. Lett.* **2005**, *30*, 2010.
(36) Koziński, M.; Garrett-Roe, S.; Hamm, P. *Chem. Phys.* **2007**, *341*, 5.
(37) Faeder, S. M. G.; Jonas, D. M. *J. Phys. Chem. A* **1999**, *103*, 10489.
(38) Nystrom, R. F.; Brown, W. G. *J. Am. Chem. Soc.* **1947**, *69*, 2548.
(39) Shine, H. J.; Zmuda, H.; Kwart, H.; Horgan, A. G.; Brechbiel, M. *J. Am. Chem. Soc.* **1982**, *104*, 5181.
(40) Schwyzer, R.; Sieber, P.; Zatsko, K. *Helv. Chim. Acta* **1958**, *41*, 491.
(41) Li, C. H. *Chem. Abstr.* **1963**, *59*, 10239e.
(42) Carpino, L. A. *J. Am. Chem. Soc.* **1993**, *115*, 4397.
(43) Tokmakoff, A. *J. Phys. Chem. A* **2000**, *104*, 4247.
(44) Kubo, R. *Adv. Chem. Phys.* **1969**, *15*, 101.
(45) Schmidt, J. R.; Sundlass, N.; Skinner, J. L. *Chem. Phys. Lett.* **2003**, *378*, 559.
(46) Oxtoby, D. W. *Adv. Chem. Phys.* **1979**, *40*, 1.
(47) Lazonder, K.; Pshenichnikov, M. S.; Wiersma, D. A. *Opt. Lett.* **2006**, *31*, 3354.
(48) Ishikawa, H.; Kim, S.; Kwak, K.; Wakasugi, K.; Fayer, M. D. *Proc. Natl. Acad. Sci. U.S.A.* **2007**, *104*, 19309.
(49) Peterson, K. A.; Rella, C. W.; Engholm, J. R.; Schwettman, H. A. *J. Phys. Chem. B* **1999**, *103*, 557.
(50) Woutersen, S.; Mu, Y.; Stock, G.; Hamm, P. *Proc. Natl. Acad. Sci. U.S.A.* **2001**, *98*, 11254.
(51) Kobus, M.; Nguyen, P. H.; Hamm, P.; Stock, G. To be submitted.

JP904905D